Applied Catalysis B: Environmental 184 (2016) 381–396

Contents lists available at ScienceDirect

Applied Catalysis B: Environmental

journal homepage: www.elsevier.com/locate/apcatb

One-pot oxidation of cellobiose to gluconic acid. Unprecedented high selectivity on bifunctional gold catalysts over mesoporous carbon by integrated texture and surface chemistry optimization

K. Morawa Eblagon*, M.F.R. Pereira, J.L. Figueiredo

Laboratório de Catálise e Materiais (LCM), Laboratório Associado LSRE/LCM, Departamento de Engenharia Química, Faculdade de Engenharia, Universidade do Porto, Rua Dr. Roberto Frias s/n, 4200-465 Porto, Portugal

ARTICLE INFO

Article history:
Received 13 July 2015
Received in revised form
29 September 2015
Accepted 6 October 2015
Available online 17 October 2015

Keywords:
Bifunctional catalyst
Biomass
Cellobiose
Carbon xerogel
Functionalization

ABSTRACT

Bifunctional catalysts coupling acid sites for activation of glycosidic bond via hydrolysis with metallic sites for further oxidation of glucose intermediate offer an advanced technological solution toward direct conversion of cellulose to platform chemicals. Gold (metallic functionality) was supported on pristine and functionalized mesoporous carbons including; carbon xerogels (CXs) with distinct morphologies and ordered mesoporous carbons (OMCs). Phenolic groups (acidic sites) were introduced on the surface of these carbons by air treatment, which was confirmed by XPS, TPD and IR results. The bifunctional Au catalysts were applied in the direct tandem oxidative conversion of cellobiose to gluconic acid. A remarkably high selectivity of nearly 80% to gluconic acid was obtained in a short reaction time of only 75 min using Au catalyst supported on functionalized CX presenting larger average mesopores size. The adsorption of the substrate (cellobiose), intermediate (glucose) and product (gluconic acid), influenced by the polarity of the carbon support, was found to have a significant effect on the selectivity to gluconic acid. The combined effect of the adequate texture and surface chemistry of the support played a vital role in the performance of the bifunctional catalyst in this process. It was proposed that a conformational change in cellobiose exposing glycosidic bond for hydrolysis, was induced upon adsorption in the larger mesopores of CX, leading to higher selectivity to glucose. On the other hand, the phenolic groups on the carbon surface played a double role as binding sites for cellobiose and as catalytic sites for the selective hydrolysis of cellobiose to glucose. The tandem reaction and its consecutive steps (cellobiose hydrolysis and glucose oxidation) were modeled, and the rate constants were derived and compared. The oxidation of glucose by Au nanoparticles was found to take place directly on the surface of the bifunctional catalysts without desorbing to the reaction medium. The present findings contribute to the advancement in understanding of the role of carbon acidic groups in the catalytic performance of bifunctional carbon supported gold catalysts in one-pot tandem reactions of biomass valorization.

1. Introduction

Great efforts are paid around the globe to the development of new, economically viable and environmentally friendly technologies which allow converting lignocellulosic biomass into renewable fine chemicals and fuels [1]. Cellulose is the most abundant non-edible source of carbon, constituting 40–50% of biomass composition by weight [2]. Cellulose can yield versatile platform molecules, however, its direct utilization proves challenging due to its very robust structure. On the other hand, cellobiose is a dimer of glucose connected by β-1,4-glycosidic bond which is soluble in water and represents a simple model molecule to study the conversion of cellulose [3]. In this regard, the study of catalytic systems for conversion of cellobiose can undoubtedly provide helpful insights for the development of more sophisticated catalytic systems for valorization of cellulose.

The processing cost, to convert biomass into useful products can be significantly decreased by employing multistep reactions carried out by cascade catalysis without the need for a recovery step of the intermediate products. For example, cellulose can be converted to value-added chemicals using bifunctional catalysts in one-pot tandem reaction, which can increase the overall efficiency and product selectivity. Following this strategy by coupling acid sites for hydrolyzing the glycosidic bonds in cellulose and metal sites for

* Corresponding author.
E-mail address: keblagon@fe.up.pt (K. Morawa Eblagon).

http://dx.doi.org/10.1016/j.apcatb.2015.10.011
0926-3373/

subsequent oxidation, it is possible to obtain gluconic acid directly from cellulose/cellobiose in water under O_2 pressure. Gluconic acid is an important chemical with an estimated market of 60,000 t per year, which is used as chelating agent, food additive, cleanser and versatile intermediate in the pharmaceutical, polymer and cosmetics industries [4,5]. Thus far, only a limited amount of studies were focused on the direct conversion of cellulose/cellobiose to gluconic acid combining hydrolysis and oxidation reactions. Among the limited works, very promising results in one-pot production of gluconic acid from cellobiose were obtained using gold nanoparticles supported on pristine and nitric acid functionalized multiwall carbon nanotubes [5], or on Keggin-type polyoxometalates [3,6], where the improved selectivity to gluconic acid was attributed to the acidity of the supports. Recently, a unique metal-support interaction between Au and TiO_2 was found to result in excellent catalytic activity and high gluconic acid yield in this tandem process [7]. Promising results were also obtained using bimetallic Cu–Au/TiO_2 catalyst [8]. Limited activity was also reported in this cascade reaction on Pd grafted on carbon xerogels [9] and Pt supported on sulfonated carbon [10]. Nevertheless, there is a constant need to research new catalysts based on easily accessible and cheap materials such as mesoporous carbon for application in sugar acids production directly from cellobiose/cellulose.

Mesoporous carbon based materials have attracted much interest as high performance catalysts for aqueous phase conversion of biomass, mainly due to their adequate structural integrity [11] and suitable texture. Additionally, they were found to adsorb cellulosic molecules (β-glucans) more effectively in comparison to metal oxides [12]. For example carbon xerogels have been successfully applied as electrode materials in supercapacitors and fuel cells, supports in electrochemistry [13,14] and catalysis [9,15]. In this respect, synthetic carbonaceous materials like carbon xerogels (CX) and ordered mesoporous carbons (OMC) can be considered attractive alternative supports to CNT mainly due to their significantly lower cost. Moreover, these materials offer a remarkable potential for designing and tailoring their textural and surface properties to fit the specific application needs [16]. With this regard, here we report for the first time the influence of the textural properties and surface chemistry of mesoporous carbon supports for Au bifunctional catalysts on the catalytic performance in oxidative conversion of cellobiose to gluconic acid. To our best knowledge, gold supported on CXs or OMC has not been yet reported for this tandem process. The kinetics of cascade hydrolytic oxidation of cellobiose was modeled here for the first time and the rate constants of the intermediate reactions were calculated. The study of bifunctional catalysts presented here lays the groundwork for exploring other environmentally friendly processes for transformation of cellulose into platform chemicals and/or fuels.

2. Experimental

2.1. Synthesis and functionalization of carbon supports

Two carbon xerogels with distinct porosities were prepared by polycondensation of resorcinol with formaldehyde (1:2 M) in water, adapting a procedure reported in the literature [17]. In brief, 25 g of resorcinol (Aldrich, 99%) was dissolved in 47 mL of deionized water. Subsequently, 34 mL of formaldehyde (Aldrich, 37% in water, stabilized with 10–15% methanol) was added and the mixture was homogenized. In order to control the textural properties of the resulting CXs, the pH of the precursor solution was adjusted for pH 5.6 or pH 6.1 with sodium hydroxide solution. The gelation step was carried out in oil bath heated to 363 K for 72 h. Subsequently, the resulting dark gel was crushed and dried in a muffle furnace following a stepwise procedure from 333 to 393 K for 4 days. After drying, the gel was carbonized under nitrogen flow (50 cm^3/min), following a previously optimized heating program [18]. The resulting carbon xerogel prepared with a pH 5.6 was abbreviated CX5.6 and the CX prepared with a pH 6.1 was abbreviated CX6.1. The burn-off obtained after carbonization was around 50%.

Ordered mesoporous carbons were prepared by a novel soft-templating phase separation method [19]. Briefly, 3 g of resorcinol, 2.5 g of Pluronic® F-127 (Aldrich) were dissolved in 20 mL of an ethanol/deionized water solution (10:9). Next, 0.2 mL of HCl 37% was added in order to adjust the pH to 1. After 1 h of stirring, 2.3 g of formaldehyde (Aldrich, 37% in water, stabilized with 10–15% methanol) was poured into the precursor solution and the temperature was raised to 323 K. After phase separation (around 2 h), the aqueous part was discarded and the organic phase was cured at 323 K, followed by 353 K and finally 373 K with 12 h duration in each step. After drying, the resins were heated up under N_2 flow (100 cm^3/min) up to 823 K for 1 h in order to remove F127, followed by 1073 K for 2 h to fully carbonize the materials, resulting in pristine OMC. The burn-off obtained after carbonization was 76%. The synthesized mesoporous supports were compared to a commercial CNT sample (Nanocyl 3100) with purity ≥95%, diameter of 9.5 nm and average length of 1.5 μ.

Gas phase activation was employed to generate oxygen groups on the carbon supports, adapting a procedure from Ref. [9]. In short, 0.5 g of carbon material was placed inside a quartz reactor and heated up to 623 K in an oven for 3 h under air flow of 100 cm^3/min with a heating rate of 20 K/min. Prior to the functionalization treatment, the synthesized carbon materials were ground and sieved to a particle size ≤100 μm. As prepared materials designated: CX_5.6_air, CX_6.1_air and OMC_air were used as supports for gold nanoparticles.

2.2. Preparation of supported gold nanoparticles

The concentration of the gold precursor solution was adjusted so that the theoretical metal loading was 1 wt% in all cases. Wet impregnation method was chosen based on the promising results reported for this reaction using 1% Au/CNT [5]. In brief, 0.99 g of carbon support was dispersed in 20 mL of distilled water. Subsequently, 5 mL solution of 0.024 g of $HAuCl_4{\cdot}3H_2O$ (Aldrich, ≥99.9% metal basis) was added dropwise to the support slurry under sonication. The solvent was evaporated at 373 K in air, followed by reduction in H_2 flow of 50 cm^3/min, with a heating rate of 10 K/min up to 523 K for 2 h.

On the other hand, reduction at room temperature using a strong reducing agent like citric acid can decrease the risk of sintering of gold particles as well as preserve the least stable functional groups on the surface of the carbon supports. Hence, for comparison, catalysts were prepared using modified citric method [20]. In the first step, 0.99 g of carbon supports was dispersed in ultrasonic bath in 500 mL of isopropanol (JMS LDA, 99.9%). Subsequently, two solutions were prepared; 0.024 g of $HAuCl_4{\cdot}3H_2O$ and 0.02 g of citric acid (Aldrich, ACS reagent ≥99.5%) in 10 mL of isopropanol. In the next step, these solutions were simultaneously added dropwise to the suspension of the support during ultrasonication. After the addition, the resulting dispersion was vigorously stirred at 600 rpm at room temperature for 2 h. Finally, the catalysts were copiously washed first with isopropanol, followed by deionized water and dried at 373 K in the oven for 12 h.

2.3. Characterization techniques

Textural characterization of the samples was obtained by measuring N_2 adsorption isotherms at 77 K using a Nova 4200e (Quantachrome Instruments) equipment. BET surface area (S_{BET}),

mesopore surface area (S_{meso}), and micropore volume (V_{micro}) were calculated using the BET equation and applying *t*-method respectively. The volume of mesopores (V_{meso}) was calculated as follows; $V_{meso} = V_{total} - V_{micro}$. The pore size distributions were obtained using the QSDFT equilibrium method for slit/cylindrical pores.

Thermogravimetric analyses (TGA) were performed using an STA 490 PC/4/H Luxx Netzsch thermal analyzer to study the oxidation of the materials in air. The experiments were carried out by heating the samples at 5 K/min under air flow (50 cm^3/min) from 298 K up to 1173 K. Surface functional groups on the samples were investigated by temperature-programmed desorption (TPD). The TPD spectra were obtained with a fully automated AMI-300 Catalyst Characterization Instrument (Altamira Instruments) connected to a Dycor Dymaxion Mass Spectrometer. Two signals were monitored in the mass spectrometer: $m/z = 28$ (CO) and $m/z = 44$ (CO_2). For the quantification of the CO and CO_2 released during TPD, calibration of these gases was carried out at the end of each analysis. In order to determine the amount of each surface group, the deconvolution of the CO and CO_2 TPD spectra was carried out. A multiple Gaussian function was used for fitting each of the TPD spectra and the numerical calculations were based on previous work [21,22].

Infra-red spectroscopy was applied for further characterization of the surface oxygen functionalities. The FTIR spectra were recorded using a NICOLET 510P spectrometer. Typically, each spectrum was built from 256 scans at a resolution of 4 cm^{-1}. The measurements were conducted between wavenumbers of 4000 and 600 cm^{-1}.

The morphology of the samples and their qualitative composition was obtained from SEM images and EDS analysis, respectively. The SEM micrographs were recorded using a high resolution environmental scanning electron microscope (FEI Quanta 400 FEG ESEM/EDAX Genesis X4M) fitted with an X-ray microanalysis and backscattered electron diffraction pattern analysis working at 20 kV.

The as-prepared 1% Au/carbon catalysts were further characterized using a TEM CM 20 (accelerating voltage 310 and 208 kV at nominal magnification). For determination of particle size distribution, not less than 100 particles from different areas of the sample were measured, using an image analysis software (*ImageJ*).

The amount of gold in the representative catalysts was determined with an ICPOES (Vista RL, Varian) after matrix-matched calibration. Not more than 5 mg of the sample was dissolved in 2 mL of aqua regia. Finally, the solutions were diluted in 50-mL volumetric flasks and the analysis was carried out.

The electronic state of gold and oxygen was probed using X-ray Photoelectron Spectroscopy (XPS). The XPS analysis was performed using a Kratos AXIS Ultra HSA, with VISION software for data acquisition and CASAXPS and XPSPeak 4.1 software for data analysis. The analysis was carried out with a monochromatic Al K X-ray source (1486.7 eV), operating at 15 kV (90 W), in FAT mode (Fixed Analyser Transmission), with a pass energy of 40 eV for regions ROI and 80 eV for survey. Data acquisition was performed with a pressure lower than 1.0×10^{-8} mbar using a charge neutralization system. The binding energy (BE) scale was calibrated by measuring the C 1s peak (BE = 284.5 eV) as an internal standard. The accuracy of the BE values was estimated to be ±0.1 eV. After subtraction of a Shirley background, the XPS peaks were fitted using a nonlinear, least squares routine with mixed Gaussian–Lorentzian functions.

2.4. Catalytic tests

The hydrolytic oxidation of cellobiose to gluconic acid was carried out in a 300 mL batch-type stainless steel autoclave equipped with a pressure gauge. 100 mL of 12 mmol/L cellobiose (Acros Organics 98%) in milliQ water and 0.2 g of the catalyst were charged in the autoclave. Subsequently, the autoclave was flushed and charged with 5 bar of O_2 and heated to 418 K for 105 min of reaction time. The magnetic stirring, set at 600 rpm, was started after reaching the reaction temperature at time zero. Periodically, small aliquots were sampled from the reactor for composition analysis. No pH control was carried out during these tests. The hydrolysis of cellobiose was carried out under the same reaction conditions. The oxidations of glucose and gluconic were carried out under the same reaction conditions, but using 100 mL of 6 mmol/L solutions of substrates and a shorter reaction time of 90 min.

The quantitative analysis of the reaction mixtures was carried out by high performance liquid chromatography (HPLC). The chromatograph (Elite LaChrom HITACHI) is equipped with an ultraviolet (210 nm) and a refractive index detector in series. The products were separated using Alltech OA 1000 Organic acids column. 5 mM H_2SO_4 was used as a mobile phase under isocratic elution with a flow rate of 0.5 mL/min at 313 K. Quantification of reactants and products was carried out using an external standard method. The catalytic conversion, selectivity and yield of gluconic acid were calculated as shown below. The TOC content of the samples was determined using a TOC-analyzer (Shimadzu 5500A). In addition, the gas phase was analyzed qualitatively at the end of the reaction using a gas chromatograph (GC 1000 Dani) equipped with a capillary column (Carboxen 1010 Plot, Supelco) and a thermal conductivity detector (Valco Instruments Co., Inc.).

$$\text{Conversion}\,(\%) = \frac{\text{initial moles of cellobiose} - \text{moles of cellbiose in products}}{\text{initial moles of cellobiose}} \times 100\%$$

$$\text{Selectivity}\,(\%) = \frac{\text{moles of product}}{\text{moles of cellobiose converted} \times \text{theoretical number of moles of the product}} \times 100\%$$

$$\text{Yield}\,(\%) = \frac{\text{moles of gluconic acid}}{\text{initial moles of cellobiose} \times 2} \times 100\%$$

2.5. Modeling of the reaction kinetics

A simple kinetic model was derived based on the obtained profiles of concentration versus time of substrate, intermediates and products. The fitting of the obtained data to the modeled values was obtained following the step by step procedure reported previously [23]. Shortly, the differential equations were derived for each of the intermediate step of the proposed reaction model. These equations were readily solved to obtain the initial modeled concentration-time profiles of the species using the 4th and 5th order Runge–Kutta formulas with the following boundary conditions imposed: at the starting point (time = 0 [s]) the concentration of the substrate was assumed to be 100% ($[P_0] = 100$ (mole %)) and the concentrations of all other species were assumed to be zero. The first rate constant, k_0, was determined by a regression analysis of the P_0 concentration-time profile (derived from the conversion) against a first order integrated rate law as described in [24] and shown in the equation below:

$$[P_0] = [P_0]_{t=0} \exp\left(k_0\left(t + \delta\right)\right)$$

where $[P_0]_{t=0}$ represents the concentration of P_0 at the time zero (=100 mole %), whereas δ represents the correction factor for any lag time due to experimental error (determined from the regression analysis). The remaining rate constants were derived using a Nelder–Mead method (simplex method) [25]. k_1, k_2, k_3 and k_4 are the rate constants as calculated from the differential representation of the reaction equations as follows:

$$\frac{d[P_0]}{dt} = -k_0 \times [P_0] \quad (1)$$

Table 1
Textural properties of the supports and selected catalysts. S_{BET}—specific surface areas determined by the BET equation V_{total}—total pore volume obtained at $P/P_0 = 0.99$, V_{micro}—micropores volume, Pore size-QSDFT mode of the pore size distribution in nm. Citric—catalyst prepared by citric method, IMP—catalysts prepared by wet impregnation method.

Sample	S_{BET} (±10)($m^2\ g^{-1}$)	S_{meso} (±5)($m^2\ g^{-1}$)	V_{total}($cm^3\ g^{-1}$)	V_{micro} (±0.01)($cm^3\ g^{-1}$)	V_{meso} ($cm^3\ g^{-1}$)	Pore size (nm)
CNT	281	281	–	–	-	≥26
CX5.6	532	238	1.22	0.15	1.07	17, 25
CX6.1	597	264	0.99	0.17	0.82	9.2
OMC	633	322	0.56	0.16	0.40	5.2
CX5.6_air	783	306	1.64	0.24	1.40	17, 25
CX6.1_air	643	242	1.06	0.19	0.87	13
OMC_air	719	384	0.76	0.17	0.59	5.7
Au/CX5.6_citric	522	228	1.20	0.15	1.07	15,26
Au/CX5.6_air_citric	624	250	1.34	0.19	1.15	15,26
Au/CX6.1_IMP	595	248	0.94	0.16	0.78	13
Au/CX6.1_air_citric	640	280	1.14	0.19	0.95	13,16
Au/OMC_citric	514	277	0.53	0.12	0.35	4.7
Au/OMC_IMP	580	291	0.47	0.15	0.38	4.8
Au/OMC_air_IMP	704	383	0.72	0.17	0.55	5.7

$$\frac{d[P_1]}{dt} = k_1 \times [P_0] - k_3 \times [P_1] - k_6 \times [P_1] \quad (2)$$

$$\frac{d[P_2]}{dt} = k_2 \times [P_0] - k_6 \times [P_1] - k_4 \times [P_2] \quad (3)$$

$$\frac{d[P_3]}{dt} = k_3 \times [P_1] + k_4 \times [P_2] + k_5 \times [P_0] \quad (4)$$

where P_0 is the concentration of cellobiose, P_1 is the concentration of glucose, P_2 is the concentration of gluconic acid and P_3 is the sum of concentrations of the side products. The mismatch between experimental and modeled values was calculated minimizing the root mean square difference between the iteratively fitted model and the experimental data. All calculations were performed using Matlab (version 7.5). For the sake of simplicity, the side products of the reaction were lumped, which provided a good agreement with experimental data.

3. Results

3.1. Carbon supports

The texture and surface properties of the support very often play an important role in the performance of the catalysts. It is noted that the porosity of the selected carbon materials is very different as a consequence of their diverse structures. The "state of the art" carbon nanotube (CNT) support is a virtually non-porous material made of graphene sheets rolled up into cylinders with increasing diameter. The pores present in CNT are the free spaces in the CNT bundles. Carbon xerogels (CX) on the other hand, have a structure of interconnected nanosized primary spherical particles, the size of which influences their porosity and depends on the pH set during synthesis [17,26]. The micropores of these materials are situated inside the particles and the voids between nodules correspond to meso- and macro-pores (inter-particle voids). Ordered mesoporous carbons (OMC) are synthesized using an assembly of a block copolymer template with a carbon precursor, and display well-defined cylindrical pores with narrow pore size distribution and high specific surface area [27].

The textural properties of these carbon supports were characterized by nitrogen adsorption/desorption isotherms and the results are gathered in Table 1. The N_2 isotherms together with the pore size distributions can be found in Supplementary material, Fig. 1s. The measurements confirmed the predominantly mesoporous character of OMC and CXs. It should be noted that these materials have similar specific surface areas and different mesopore size. The OMC showed a unimodal and narrow pore size distribution with the lowest pore size of 4 nm. On the other hand, CX6.1 displayed larger average mesopore size (9 nm) and broader pore size distribution than OMC (see Table 1 and Fig. 1s). The pore size of CX5.6 was widely dispersed and presented the biggest size of all of the mesoporous carbons studied. In agreement with the literature, with the increase in pH during CX synthesis, the average pore size and the total pore volume decreased, but simultaneously the BET surface area, mesoporous surface area and micropores volume increased [28]. The higher total pore volume in CX5.6 as compared to that of CX6.1 is associated with the creation of bigger pores in the former, which had only small contribution to the total surface area of the material. Despite the similar BET surface area of OMC and CX6.1, the former displayed much higher S_{meso} and the largest relative contribution of micropores with respect to the total pore volume among all supports (Table 1). On the other hand, CNT due to their unique morphology showed the lowest BET surface area, as a result of N_2 being adsorbed only on the external surface of the tubes.

Another important property of carbon materials is the structural ordering of carbon. It is well established that the more structured (less defective) the carbon material is, the higher the temperature required for its gasification [29]. The corresponding curves showing the temperature of the maximum weight loss obtained by thermogravimetric analysis of the samples can be found in Supplementary material, Fig. 2s. OMC and CX5.6 showed the lowest temperature, between 860 and 870 K. CX6.1 and CNT presented a slightly higher temperature between 878 and 893 K, indicating a more stable carbonaceous structure. The different stability of carbon supports and the presence of higher concentration of defects in the structures of CX5.6 and OMC could have an influence on the functionalization step and, as a result, on the catalytic performance of the gold catalyst.

3.2. Functionalized carbon supports

The functionalization of the carbon supports in air increased the BET surface area and the micropore volume (V_{micro}) as listed in Table 1. In addition, there was a slight increase of mesoporous area (S_{meso}) in the functionalized CX5.6 and OMC samples, which can be attributed to the widening of the existing micropores during functionalization or opening of new, otherwise inaccessible pores. Comparing the contribution of V_{micro} to V_{total} of all the samples before and after functionalization, it becomes clear that the largest formation of new micropores took place during the air treatment of CX5.6 among all the supports. As a result, the percentage of V_{micro} in V_{total} increased from 12% in CX5.6 to almost 16% in CX5.6_air. In contrast, for CX6.1 the percentage of V_{micro} in V_{total} increased only marginally from 17% to 18%. This can be attributed to relatively more frail structure of the xerogels synthesized at lower pH values [30], which is in line with the lower stability of this support

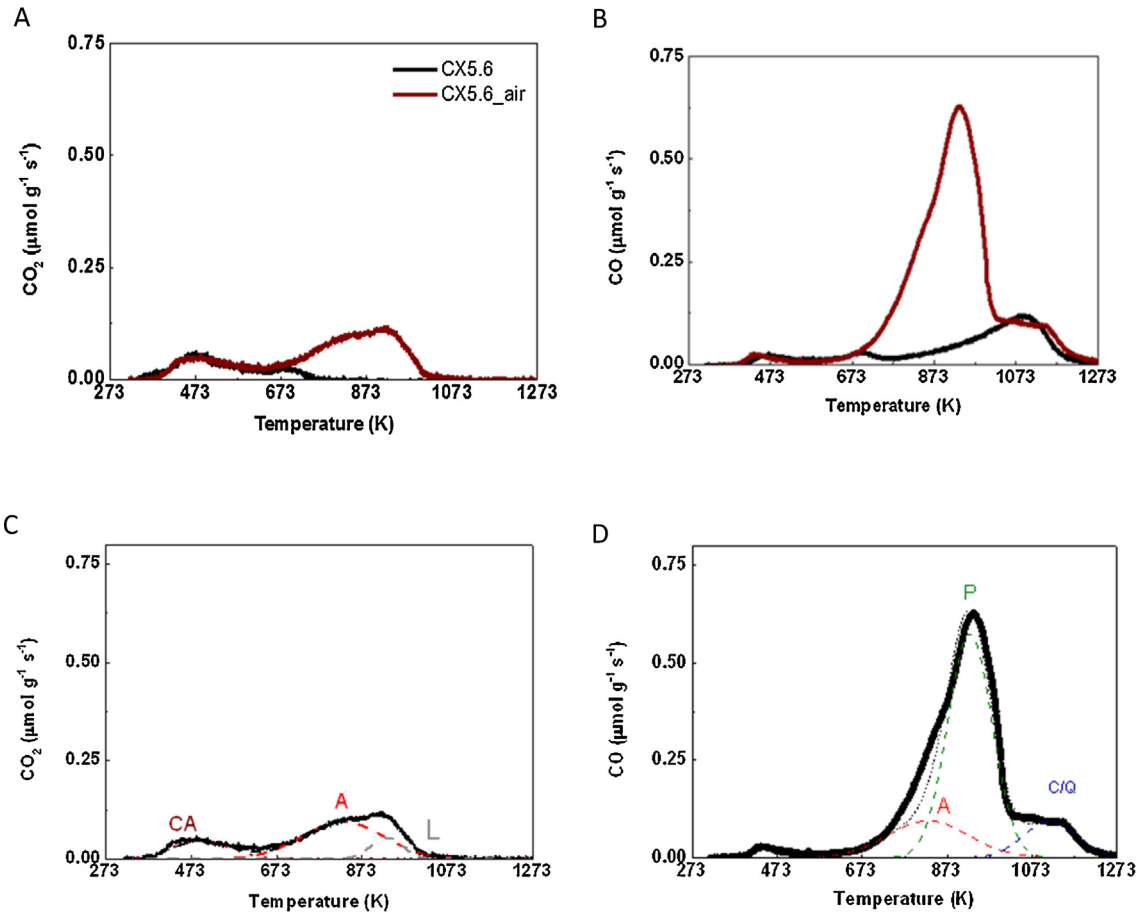

Fig. 1. Comparison of TPD spectra of pristine CX5.6 and functionalized in CX5.6_air; (A) CO_2 evolution, (B) CO evolution. Deconvolution of TPD spectra of functionalized CX5.6_air; (C) CO_2 spectrum (D) CO spectrum (CA)-carboxylic acids, (A) carboxylic anhydrides, (L) lactones, (P) phenols, (C/Q) carbonyls or quinones.

shown by the results from the aforementioned TG experiments (Supplementary material, Fig. 2s). In addition, the contribution of micropores decreased from ≈29% in OMC to 23% in OMC_air. This can be the result of broadening of the existing micropores in OMC which also agrees with the lower stability of this support (TG results). In addition, as evidenced in Table 1, the mode of pore size distribution increased in air treated samples derived from carbons with smaller pore size (OMC and CX6.1) and the pore size distribution broadened for these samples.

During the functionalization in air oxygen chemisorbs on the surface of the carbon material forming carbon–oxygen functional groups with different acidic strength. The nature and quantity of these groups, generated during treatment in air, was evaluated by temperature programmed desorption (TPD) experiments. In these measurements, the type of functional groups can be assigned by their decomposition temperature and the type of gas released (CO or CO_2). Additionally, the amount of these groups can be obtained by integration the respective component peak areas following adequate deconvolution procedures [22]. The treatment in air is expected to introduce mainly phenols, carbonyls, anhydrides and lactones, as discussed elsewhere [22].

The calculated total amounts of CO and CO_2 released during TPD experiments are gathered in Table 2. The TPD data show that the pristine xerogel samples already contain a small amount of oxygenated groups. These groups can be formed spontaneously on carbon upon exposure to the atmosphere. A comparison of CO and CO_2 TPD spectra of CX5.6 support before and after functionalization treatment is shown in Fig. 1A and B. From this figure it is clear that the quantity of oxygen functionalities was significantly increased upon treatment in air. It is interesting to note that the pristine carbon xerogels, regardless of their texture, displayed almost identical quantity of groups, as evidenced by the similar amounts of CO and CO_2 evolved upon heating during the TPD experiments (Table 2). In comparison, pristine OMC released smaller amount of CO as compared to CX samples. The total amount of gases released was also slightly higher in the case of CX. Furthermore, the ratio CO/CO_2 in CX samples decreased after the gas phase treatment, which is consistent with the higher concentration of more acidic groups, which decompose to CO_2. On the contrary, this ratio increased in OMC_air as compared to OMC. The total weight percentage of oxygen in the samples was estimated from the TPD results and it is also listed in Table 2. In general, it can be concluded that the functionalization introduced very similar overall amount of oxygenated groups, regardless of the texture of the support. Moreover, from Fig. 1, it can be noted that in the case of pristine CX5.6, there was some release

Table 2
Results of TPD analyses of carbon supports. Amounts of CO and CO_2 obtained by integration of peak areas under TPD spectra, mass percentage of oxygen estimated assuming that all of the oxygen is released as CO and CO_2.

Sample	CO (μmol g^{-1})	CO_2 (μmol g^{-1})	CO/CO_2	O_2 (wt%)
CX5.6	380	85	4.5	0.88
CX5.6_air	1464	444	3.2	3.76
CX6.1	389	88	4.4	0.90
CX6.1_air	1798	512	3.5	4.51
OMC	293	119	2.5	0.85
OMC_air	2070	417	5.0	4.65

Table 3
Results of the deconvolution of CO_2 and CO profiles using Gaussian function for carbon supports after functionalization in air. T_M—temperature corresponding to peak maximum (±20 K) in K, A_M—amount of groups in μmol g^{-1}.

Sample	CO_2						CO					
	CA		A		L		A		P		C/Q	
	T_M	A_M	T_M	A_M	T_M	A_M	T_M	A_M	T_M	A_M	T_M	A_M
CX_5.6_air	495	96	828	272	930	60	828	272	926	901	1114	174
CX_6.1_air	627	120	762	258	955	94	762	258	966	1212	1082	322
OMC_air	–	–	804	210	916	206	804	211	900	1325	1043	530

of CO at temperatures higher than the one used for carbonization of the sample (≥1070 K). Therefore, this release of CO can be partially associated with further carbonization of the xerogel matrix during the TPD measurement.

Subsequently, the TPD spectra of functionalized samples were deconvoluted in order to determine the contribution of each type of surface oxygen complex. It is noted that the mathematical procedures applied here proved to fit the experimental data very well. Fig. 1C and D shows the representative deconvolution of CX5.6_air spectrum, the results for CX6.1_air and OMC_air can be found in the Supplementary material, Fig. 3s. The CO_2 spectrum of CX5.6_air (Fig. 1C) presented less acidic carboxylic acids-CA (373–673 K) carboxylic anhydrides-A (623–853 K) and lactones-L (897–973 K). The CO spectrum of the same sample (Fig. 1D) was decomposed into three contributions, carboxylic anhydrides predetermined from the deconvolution of CO_2 spectrum, phenols (873–973 K) and carbonyl/quinones (1040–1173 K). It is noted that in the case of CX5.6_air, there might be an overlapping between the latter and the products of further carbonization of the xerogel matrix, as the release of CO at high temperature was also observed in the pristine CX5.6 sample (see Fig. 1B). It is interesting to note that the contribution of carboxylic acid groups was already observed in the pristine CX5.6 and these groups seemed to remain almost unaltered after the functionalization procedure. Similar results were reported elsewhere [31]. Table 3 shows the results of the deconvolution of all of the air treated samples, including the integrated peak areas (A) and the temperatures at peak maximum (T_M). The temperatures of the decomposition of various groups assigned here agree well with the values reported in the literature [22,28,31,32].

Comparing the data from the deconvolution of the respective TPD profiles of functionalized samples (Table 3), it can be noticed that the amounts of each type of oxygen group present in the functionalized CX is similar, regardless of their texture. In comparison to CXs, OMC_air presented significantly larger amount of lactones and carbonyl quinones and complete absence of carboxylic acid groups. This results in an overall less acidic character of this material in comparison to CXs. Most importantly, the deconvolution of the TPD spectra showed that the treatment applied here is very selective toward the introduction of large amount of phenolic groups, regardless of the type of carbon support.

Additional qualitative information about the nature of the surface oxygenated groups and associated changes in electronic state of carbon surface following the functionalization can be gained from XPS analysis. It is noted that the information obtained from XPS is distinct from that obtained in from TPD analysis in the sense that XPS is a surface method thus only the uppermost layer of the carbon material (of about 10 nm) is probed, whereas, TPD is a bulk analysis method. In the present work, XPS was employed to characterize the electronic states of carbon and oxygen in the representative CX5.6 support before and after functionalization. The results of the fitting of O 1s XPS spectra of CX5.6 and CX5.6_air are summarized in Table 4, together with the approximate amount of oxygen on the surface. The oxygen contents calculated from XPS characterization are higher for both materials, but importantly they follow the same trend as evidenced earlier by TPD results. Small

Table 4
Deconvolution of XPS bands of O 1s and derived oxygen content for carbon xerogels. (%)—intensity percentage.

Sample	BE (eV)	Peak assignment	(%)	O_2 (wt%)
CX5.6	531.1	C═O (carbonyls/quinones)	3.3	3.4
	532.4	C—O (phenols)	21.6	
	533.2	C—O (anhydrides)	20.1	
	533.9	Carboxylic groups	50.7	
	534.7	Adsorbed H_2O	4.3	
CX5.6_air	530.9	C═O (carbonyls/quinones)	9.4	6.5
	531.9	C—O (phenols)	40.7	
	533.3	C—O (anhydrides)	26.5	
	533.9	Carboxylic groups	16.6	
	534.6	Adsorbed H_2O	6.8	

differences in the distribution of the groups can be attributed to the deconvolution of the overlapping peaks in both of the methods which are influenced by the software inputs. Importantly, in the present work, the deconvolution of the evolved CO and CO_2 peaks was done applying some assumptions, which have been validated both experimentally [22] and by theoretical calculations [34]. Comparison of XPS and TPD results shows that a large amount of oxygenated groups was introduced to the external surface of the carbon xerogel as compared to its bulk, suggesting that the oxidation process applied here was somehow heterogeneous in nature. Nevertheless, this is common in case of majority of porous carbon materials [22,31,33]. High resolution O 1s XPS spectra of CX5.6 and CX5.6_air (Supplementary material, Fig. 4s) showed the coexistence of five components in agreement with the literature reports [31,35]. The curve fitting identified the following oxygen species before and after functionalization of CX5.6 support; C═O bonds in carbonyls and quinones (530.8–531.1 eV), C—O oxygen in phenols (532.1–532.6), C—O oxygen in anhydrides (533.2–533.5 eV) and carboxylic groups (533.9–534.5 eV) and finally adsorbed water (534.7–535.0 eV). Importantly, the attained oxidation is apparent by the significantly different line shape of XPS O 1s spectrum of CX5.6_air as compared to that of CX5.6 (Supplementary material, Fig. 4s). After oxidation, the XPS O 1s spectrum fitting showed that the surface of the samples became predominantly enriched in phenols, with an estimated double amount of these groups on the carbon surface. In addition, there was also a noticeable increase in contributions from carbonyl/quinones and carboxylic anhydrides, confirming the results obtained from the deconvolution of the TPD profiles (Fig. 1).

The presence of the oxygen complexes in functionalized samples was further confirmed by FTIR spectra. A clear difference can be observed comparing the spectra of the treated and untreated supports as shown in Fig. 2. In the pristine samples, two main features could be distinguished. In the range of 900–1160 cm^{-1} a series of overlapping bands was present, which was assigned to stretching vibrations of C—OH and O—H of phenol and carboxyl structure, carboxylic acids and/or carboxylic anhydrides. The other pronounced band was found in the region of 1450–1630 cm^{-1} which could be assigned to associated C═C aromatic stretching or/and carbonyl stretching vibrations of quinones or ceto-enol groups [36]. This

band is more pronounced in the case of CX5.6 (Fig. 2A) and OMC (Fig. 2C). In fact, some release of CO at higher temperatures was observed in the TPD spectra (see Fig. 1B) of these samples, which could suggest the presence of quinones. After the oxidation treatment, a new band arose in the region 1660–1790 cm^{-1}, which directly indicated the formation of surface oxygenated groups and is characteristic of C=O stretching vibration of the carbonyl group [37]. Moreover, as a result of functionalization, the band in the region of 900–1160 cm^{-1} increased in intensity and broadened. This band can be assigned to C—O stretching in surface phenols, hydroquinones, lactones and carboxylic anhydrides [22,38,39]. Similar changes were observed in the region of 1450–1630 cm^{-1}. In the functionalized samples, the intensity of this band increased drastically and the band broadened, mainly due to the introduction of quinones as evidenced by XPS (see Table 4). Comparison of TPD, XPS and IR results showed a pronounced difference in the chemical surface characteristics between the pristine and functionalized supports. It was clearly evidenced that the functionalization in air applied in the present work increased the amount of mainly phenols among other species on the surface of mesoporous carbons.

3.3. Gold catalysts

Based on the literature reports, the acid–base properties of the support mainly play a role in the first step of this tandem reaction, which is the hydrolysis of cellobiose to glucose [3,5,7–9]. Nevertheless, the presence of the oxygenated functional groups on the surface of carbon can affect the deposition of gold and as a result the second step of the studied reaction, the oxidation of glucose to gluconic acid. It was reported previously that surface oxygen groups can act as anchors to metallic precursors, resulting in smaller and better dispersed nanoparticles with enhanced catalytic performance [9,31,40–42]. Thus, in order to link the catalytic performance with the properties of the mesoporous support, a detailed characterization of the selected 1 wt% Au catalysts prepared by wet-impregnation and citric method on both functionalized and pristine supports was carried out.

3.3.1. Physicochemical characterization of Au/C catalysts

As can be seen by comparison of values in Table 1, the BET surface area of carbon supports decreased upon deposition of metal. This response is attributed to the partial blockage of the microporous structure of these materials. Interestingly, in the case of Au deposited on CX6.1, OMC and CX5.6_air, a drop of BET surface area was accompanied by a gradual decrease in the mesoporous area, total pore volume and micropore volume. It is noted that the drop of these parameters was mostly pronounced in case of Au supported on CX5.6_air. This suggests that the Au particles are partially blocking micropores and a part of mesopores/macropores on this support. In fact, partial blockage of the bigger mesopores can lead to the formation of narrower mesopores, which is in agreement with the change in average pore size observed in CX5.6_air, CX5.6 and CX6.1 and OMC. In case of Au deposited on CX6.1_air, the mesoporous surface, total pore volume, mesoporous volume and average pore size increased, which is consistent with the blocking of macropores of this support by gold particles and thus creating new mesopores. Interestingly, in the case of OMC_air, besides the small drop in BET surface area, the other parameters (see Table 1) remained unaltered after deposition, pointing again to the preferential deposition of the gold nanoparticles on the external surface of this material.

The electronic state of deposited gold was studied by XPS. Fig. 3 depicts a representative high resolution spectrum recorded for 4f photoelectrons of the Au_CX56_air_citric catalyst. The XPS spectra of the remaining catalysts can be found in Supplementary material, Fig. 5s. As it can be seen, similar results were obtained for all of the catalysts studied here, suggesting that the electronic state of gold is neither affected by the support properties nor by the gold deposition method. The physicochemical characteristics, including the XPS binding energy (BE) of gold for selected samples, are gathered in Table 5. All of the Au 4f XPS spectra of the catalysts were successfully fitted with a doublet assigned to metallic gold [3,5,7]; at BE of the Au $4f_{7/2}$ (84.0–84.1 eV) and the second one Au $4f_{5/2}$ at the BE values (87–88 eV). The inspection of XPS peaks of O 1s (Supplementary material, Fig. 4s) and Au 4f (Fig. 3) of AuCX5.6_air showed no modulation of the electronic structures on the interface, thus, neither formation of strong chemical bond between Au and oxygen atoms nor strong metal-support interaction were present. The atomic percentage of gold exposed on the surface was calculated taking into account the relative intensities of Au and C in the XPS spectrum, normalized by the appropriate sensitivity factors (Table 5). The results indicate that in the catalysts supported on pristine carbon xerogels prepared by citric method, most of the gold nanoparticles are embedded in pores of the support and are not "seen" by XPS. In comparison, a significantly higher percentage of Au on the surface was obtained in catalysts prepared by wet-impregnation method on pristine supports. This can be the result of the fact that the solution of gold precursor could not sufficiently wet the pores of the hydrophobic CXs. It is worth noting that a very low exposure of gold was also obtained on Au_CNT with measured loading of 0.9 wt% (from ICP) close to the theoretical value of 1% (Table 5). Overall, the surface exposure of gold on OMC was the highest, which shows that the preferential deposition of Au on this support is on its external surface, in good agreement with the obtained BET results. Further, from Table 5, it is clear that the deposition of gold is governed by the presence of oxygen functionalities. A significantly higher exposure of gold on the surface was noted for Au supported on CX and OMC containing weak acidic sites (phenol groups), taking into account that the amounts of incorporated gold (Au at% in Table 5) were virtually the same in the case of pristine or functionalized CX. As discussed before, there was no evidence in the XPS spectra of the presence of any covalent bonds involving gold and hydroxyl groups on the surface of functionalized carbon supports. As a result, it can be assumed that the OH groups on the surface of carbons are coordinating with the Au^{+3} ions from the solution by simple electrostatic interaction. In fact, it has been lately demonstrated that the adhesion and nucleation of Au on functionalized graphite is indeed at surface hydroxyl groups [43]. The higher exposure of gold on functionalized CXs can also be explained by a greater density of defects created during the air treatment of these supports. These defects can trap Au atoms and act as nucleation sites for Au particle formation which leads to a

Table 5
Physicochemical characterization of gold catalysts supported on pristine and functionalized carbon supports. BE $4f_{7/2}$—binding energy of Au 4f core level, Au/C (at%)—percentage of exposed surface gold species from XPS and d_{TEM}—particle size (nm) from TEM measurements.

Sample	[a] BE $4f_{7/2}$(eV)	Au/C (at %)[b]	Au (wt%)[c]	d_{TEM}(nm)[d]
Au/CX6.1_citric	84.1	0.03	0.80	18.3
Au/CX5.6_citric	84.1	0.02	0.88	13.3
Au/OMC_citric	84.1	0.35	0.75	31.5
Au/CX6.1_IMP	84.1	0.07	0.57	16.9
Au/CX5.6_IMP	84.1	0.11	0.78	14.1
Au/OMC_IMP	84.1	0.50	0.67	28.4
Au/CNT_IMP	84.0	0.01	0.90	10.9
Au/CX6.1_air_citric	84.1	0.13	0.80	14.9
Au/CX5.6_air_citric	84.1	0.24	0.87	12.2
Au/CX5.6_air_IMP	84.0	0.07	n/a	n/a
Au/OMC_air_IMP	84.1	0.10	n/a	n/a

[a] BE $4f_{7/2}$ (eV) Binding energy of Au 4f core level.[b] Au/C (at%) percentage of exposed surface gold species, determined by the areas of the respective bands in the high resolution XPS.[c] Gold loading (ICP).[d] Average diameter of the particles (TEM).

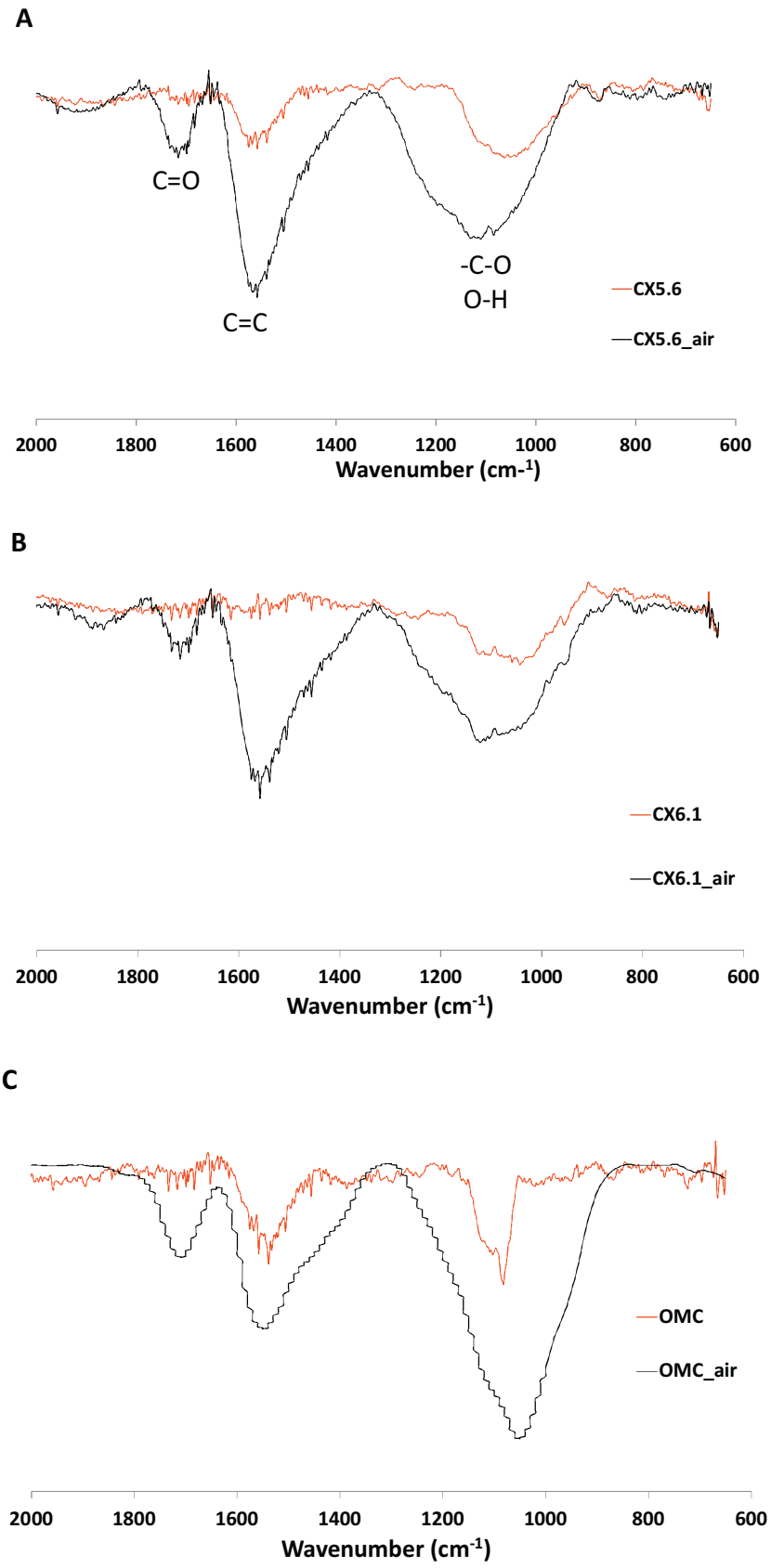

Fig. 2. Part of the FTIR spectra recorded for carbon supports before and after functionalization.

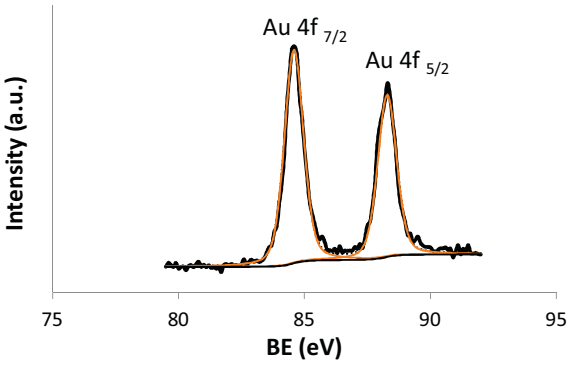

Fig. 3. Au 4f XPS spectrum of Au/CX5.6_air_citric.

higher exposure of gold on the edges of the basal plane of carbon surface, which is in close vicinity to the surface phenolic groups.

Further, it is worth noting that the actual metal loadings (ICP measurements) are very close to the theoretical 1% in case of catalyst prepared by citric method on pristine and functionalized CXs. Interestingly, despite the chemical inertness and very regular structure, 0.9% of gold was successfully anchored without any pretreatment on the surface of carbon nanotubes by wet-impregnation method. On the contrary, significantly lower amount of gold was incorporated in the catalysts prepared by wet-impregnation on pristine CXs (Table 5). This result can be associated with the surface charge developed on the carbon supports upon immersing in water [44]. For the depositions carried out in aqueous media, the pH value plays a key role in controlling the actual distribution of gold (III) species and the net charge of the solid support surface. Thus, the surface of carbon is neutral at the pH value known as point zero charge (pzc). Subsequently, when pH < pzc, the surface charge will be positive, and will adsorb anions. The pzc of pristine CX5.6 was measured to be at pH 7.7. In addition, the pH of the solution of auric acid in water was measured to be pH 2.7 and dropped to pH 1.5 upon addition of citric acid. Hence, it is speculated that at lower pH, the interaction between gold species in the solution and the carbon support is more favorable leading to higher final Au loadings obtained by the citric method. In addition, the poor surface chemistry of OMC and small pore size which was inaccessible to the precursor solution resulted in low loadings of gold obtained on OMC, regardless of the deposition method.

The energy dispersive X-ray spectroscopy (EDS) carried out on a single supported particle confirmed the presence of gold on carbon (Fig. 4B). Further, TEM and SEM images showed that the dispersion of the particles obtained by both methods was rather broad, with an average particle size larger than 10.9 nm, but also containing agglomerates of up to 100 nm as evidenced in the particle size distributions in Fig. 4A, C and D. Individual bigger particles were especially visible on OMC support (Fig. 4E), which had the smallest pore size of all of the materials studied here. In general, smaller average particle size was obtained on supports with larger voids (Table 5). The catalysts typically consisted of smaller spherical particles (circled in Fig. 4C) of gold; however, some larger faceted particles can be clearly seen on SEM images (Fig. 4B, E and F). Most importantly, the functionalization of CX decreased the average particle size of Au by improving the adsorption of the gold precursor (as discussed above) and preventing agglomeration. The average Au particle size obtained here can appear rather large taking into consideration that high surface area supports were used in combination with low metal loadings. Nevertheless, this can be attributed to both the nature of gold itself and the surface properties of the carbon. Gold has a much lower melting point than for example platinum (1337 K versus 2041 K) which makes gold nanoparticles very mobile and susceptible to sintering. Furthermore, it is known that gold has much lower affinity to carbon supports than to metal oxides and this is due to the carbon surface being hydrophobic in nature and containing a much lower density of surface hydroxyl groups as compared to metal oxides. Additionally, our results showed, in agreement with the literature, that citrate capping molecules do not effectively passivate the surface of the newly formed Au nanoclusters to sufficiently prevent their subsequent growth, resulting in larger Au particles [20,45]. Concerning the wet-impregnation method, the residual chloride species from the precursor might have favored further Au aggregation during thermal treatment by promoting the mobility of gold atoms which led to higher particle size. Nevertheless, in the case of the reactions in which the anticipated product is an intermediate species like oxidation of cellobiose to gluconic acid, a larger particle size can lead to higher selectivity due to the fact that these particles tend to be less active for subsequent oxidation of the product. This trend has been already observed in glycerol oxidation to sodium glycerate on Au supported on carbon [46].

3.4. Direct catalytic oxidation of cellobiose to gluconic acid

The one pot hydrolytic oxidation of cellobiose entails the hydrolysis of cellobiose to glucose (mainly on the carbon support) and its subsequent selective oxidation (on supported Au nanoparticles) to form gluconic acid as shown in Fig. 5. The former step involves the breaking of the β-(1,4)glycosidic linkage between two glucose monomers. With respect to the oxidation step, it should be noted that glucose contains five types of bonds, out of which three display similar bond energies: C—C, C—H and C—O. Consequently, the hydrolysis/oxidation of cellobiose in one pot is a complex process which inevitably implicates a number of side-reactions affording a wide range of by-products not only from hydrolysis of cellobiose, but also oxidation, dehydration, rehydration and cracking of cellobiose, glucose and other unidentified intermediates. In the present work, besides glucose and gluconic acid, much smaller quantities of glyceric acid, glycolic acid, succinic acid, formic acid and acetic acid were observed among other unidentified products. Similar products of this reaction were previously reported on Au/CNT [5] and Au/TiO_2 [8]. Some traces of fructose (max selectivity ≈3%) from the isomerization of glucose were also detected in our work, depending on the catalyst used. It is noted that the carbon balance obtained from the comparison of the moles of carbon derived from concentrations measured by HPLC and the conversion from TOC analysis was between 85–90%, depending on the catalyst, indicating the presence of some gaseous products. CO_2 was identified to be a main gaseous end-product and its concentration rose with increased conversion. In accordance with the literature reports, the CO_2 in our case can be the product from glucose oxidation to formic acid as well as the decomposition of acetic acid, glyceric or glycolic acids [8,47]. In addition, degradation of gluconic acid to a lower aldonic acid can produce CO [48] which can be easily converted to CO_2 on gold nanoparticles. The geometry of the products structure which were commonly observed in all of the catalysts tested was calculated using Gaussian software (Gaussian 03, revision C.02. Wallingford, CT: Gaussian, Inc., 2004.) and the results are shown in Fig. 5.

3.4.1. Catalytic results

One pot direct conversion of cellobiose to gluconic acid was performed using 1% Au loaded on pristine and functionalized CX (CX5.6 and CX6.1), ordered mesoporous carbon (OMC) and pristine carbon nanotubes. The changes in concentration of products and intermediates within 105 min of reaction were followed. A typical selectivity versus time profile obtained for Au/CX5.6_citric can be found in Supplementary material, Fig. 5s. As it is clear from the aforementioned profile, gluconic acid is an intermediate product

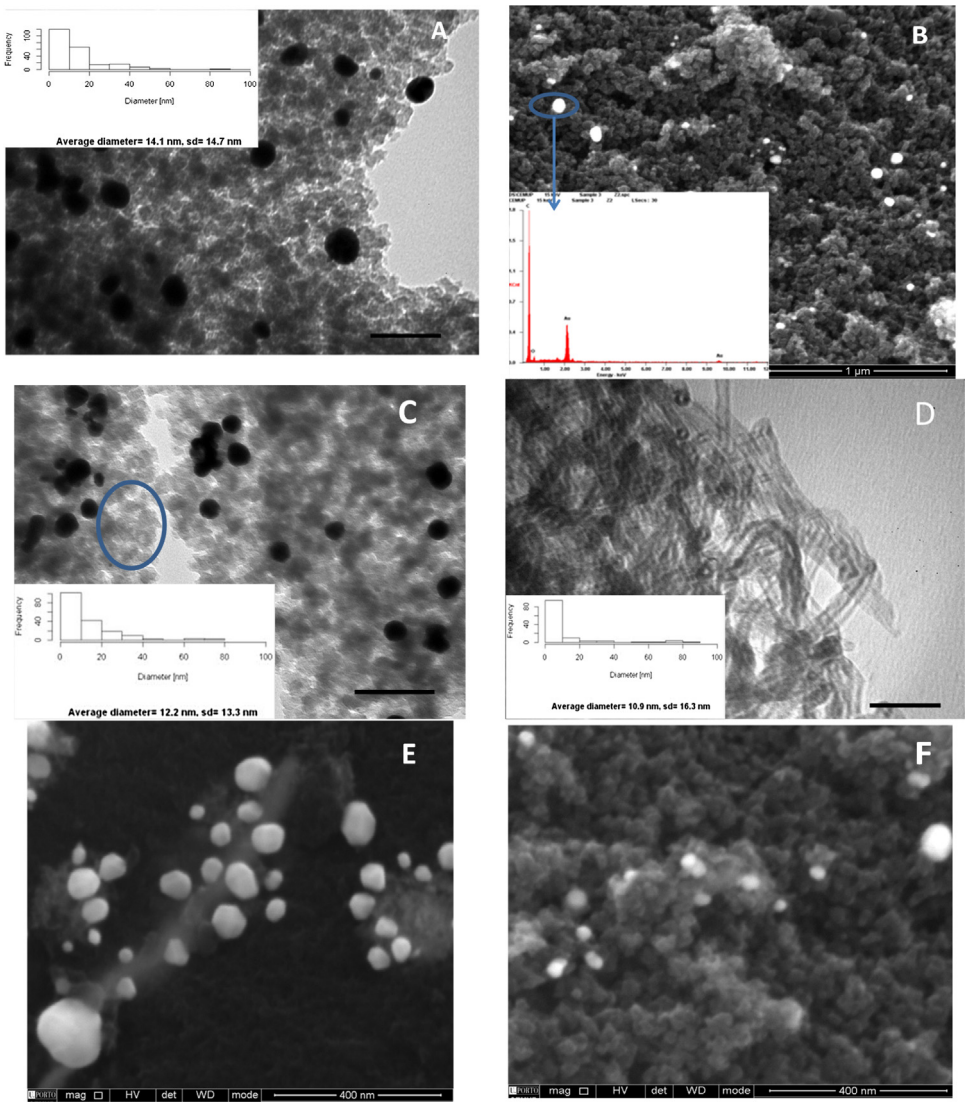

Fig. 4. (A) TEM image of Au/CX5.6_IMP, inset; a corresponding particle size distribution, scale bar = 50 nm (B) SEM image of the Au/CX5.6, inset; EDS spectra of the marked region of the same sample, (C) TEM image of Au/CX5.6_air_citric, inset; a corresponding particle size distribution, circled area with smaller Au nanoparticles, scale bar = 50 nm (D) TEM image of Au/CNT_IMP, inset; a corresponding particle size distribution, scale bar = 50 nm (E) SEM image of Au/OMC_citric, (F) SEM image of Au/CX5.6_citric_air.

in this cascade process and as such it is prone to undergo further conversion/degradation. For this reason, it is believed that comparing the catalytic results at a fixed amount of time might not reveal the full potential of the tested catalysts. Therefore, in the present work, the catalytic results were compared taking into account the maximum yield of gluconic acid obtained during 105 min of the reaction. Hence, the comparison of catalytic results including yields and selectivity to gluconic acid and conversion of cellobiose is shown in Fig. 6. Detailed selectivity at the point of maximum yield of gluconic acid and the time of the reaction required to obtain maximum yield can be found in Supplementary material, Table 1s. Even though the highest yield of gluconic acid was obtained on Au supported on the "state of art" CNT [5], all of the tested Au catalysts supported on mesoporous carbons were able to efficiently convert cellobiose to gluconic acid in a remarkably short time (less than 90 min as compared to 3 h [5]) and with acceptable selectivity (Supplementary material, Table 1s). Most interestingly, Au supported on functionalized xerogel (Au_CX5.6_air) showed not only comparable performance to Au/CNT, but also reached a remarkable selectivity of almost 80% to gluconic acid in only 75 min of the reaction. This is less than half of the time usually reported in the literature to obtain the best selectivity to gluconic acid in this process [5,3], under otherwise similar reaction conditions. To our best knowledge, this is by far the highest selectivity reported in this tandem reaction using gold supported on carbon, and higher than that recently obtained on Au/TiO_2 [7].

Another intriguing finding is that the selectivity of gluconic acid was remarkably improved by functionalization in air and importantly this appeared to be true for all of the catalytic systems tested here, regardless of the textural properties of the support. It should be noted that higher yields of gluconic acid were obtained on the functionalized supports even taking into consideration the slight differences in metal loading between the catalysts (see Table 5). With respect to correlating the catalytic performance with textural properties listed in Table 1, it is clear that the yield of gluconic acid obtained is higher for gold supported on carbon materials with bigger voids, following the trend CNT > CX56 > CX61 > OMC. In addition, the selectivity to gluconic acid also followed the same pattern, being the highest on the support with biggest pores. Because gluconic acid is an intermediate product of this tandem reaction, it appears that the size of the pores can have a direct influence on the mode/geometry of adsorption of cellobiose on the surface of these catalysts. Bigger pores can render glycosidic bonds in cellobiose more accessible for activation influencing the final selectivity of the

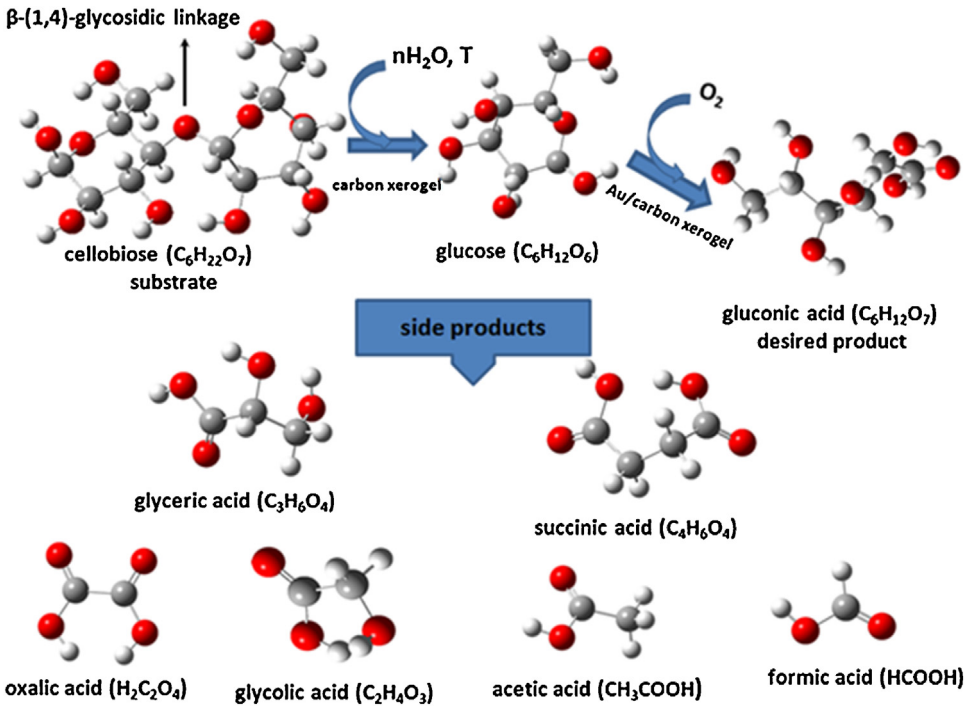

Fig. 5. The general scheme of the steps involved in the tandem conversion of cellobiose to gluconic acid. Hydrolysis of cellobiose to glucose over carbon support, followed by oxidation of glucose on the surface of supported gold nanoparticles. The theoretical structures of products of oxidative hydrolysis of cellobiose to gluconic acid as identified in the present work using HPLC were calculated with the aid of Gaussian. The glycosidic linkage between two glucose monomers in cellobiose is clearly marked.

reaction. Another possibility is that the drop in maximum selectivity to gluconic acid on the supports with smaller pores can be the result of impaired desorption of gluconic acid from the surface of the supports due to diffusion limitations in their pore texture. This can lead to unwanted by-products which can be produced through subsequent oxidation and fragmentation of gluconic acid. In addition, it is certain that the performance of the catalyst was influenced by the method of gold deposition. In general, citric method would be preferable over wet impregnation for the preparation of Au supported on mesoporous carbon for application in this tandem process. This is due to the fact that reduction with citric acid afforded higher metal loadings (Table 5), which makes it economically more attractive, even though the obtained conversions at maximum selectivity to gluconic acid per gram of gold present on the surface would be slightly lower in comparison to the catalysts prepared by wet impregnation. It should be noted that both methods resulted in a similar gold particle size, despite differences in Au loading (see Table 5). On the other hand, the oxidation of glucose was claimed to be a structure-sensitive reaction [49] and it was emphasized that for an effective oxidation of glucose, Au particles should be below 5 nm [5,6,50]. On the contrary, our results show that in the case of hydrolytic oxidation of cellobiose to gluconic acid, the size of Au nanoparticles does not play a decisive role in the observed activity trends. Careful inspection of Fig. 6 and Table 1s in Supplementary material revealed that almost 100% conversion of cellobiose in just 90 min were obtained using Au_OMC_citric

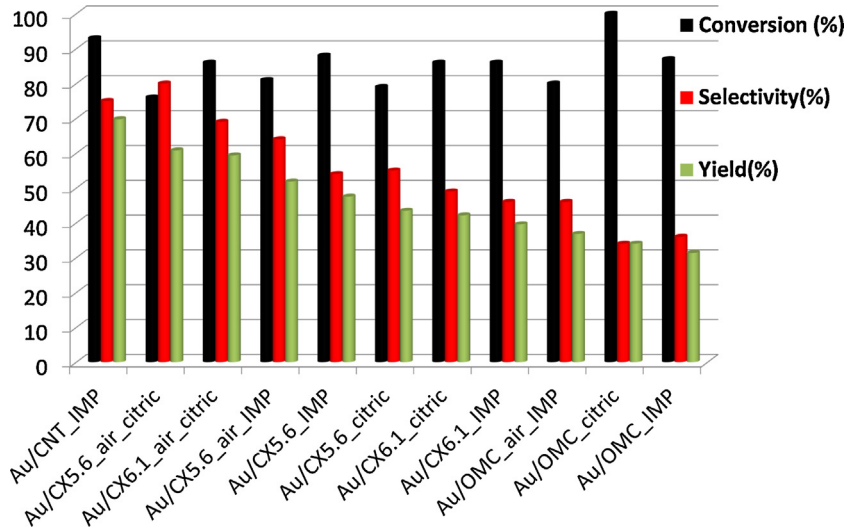

Fig. 6. Catalytic performances of 1 wt% Au catalysts loaded on pristine and functionalized carbon materials. Reaction conditions: T = 418 K, 100 mL of 12 mM/L of cellobiose in water, time: maximum 105 min, $P(O_2)$ = 5 bar.

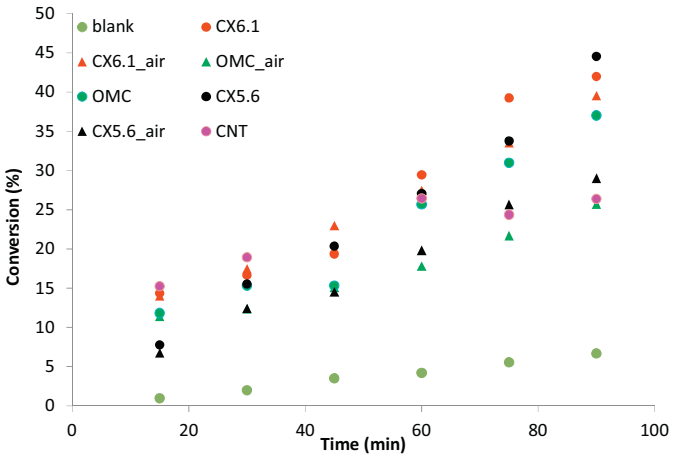

Fig. 7. Conversion of cellobiose in time over pristine and functionalized carbon supports. Blank-experiment without catalyst.

catalyst, which had the highest particle size from all of the materials studied here (Table 5). Moreover, 91% conversion of cellobiose in 3 h was reported for Au supported on multiwalled carbon nanotube with average particle size of 5.8 nm [5]. In comparison, in the present work, Au/CNT with average particle size of 10.9 nm afforded 93% conversion in just 60 min under otherwise very similar reaction conditions to those used in [5]. Hence, in the light of these results, no direct correlation could be established between Au average particle size and the activity of the catalyst in this tandem reaction. Nevertheless, it should be kept in mind that the dispersion of the particle size in the present work was rather broad (see Fig. 4); therefore the actual influence of the particle size could be partially masked. Overall, the results strongly suggest that the performance of Au supported catalysts in direct one-pot conversion of cellobiose to gluconic acid is mainly dependent on the chemistry and textural properties of the support.

3.4.2. *Influence of the support properties on the reaction mechanism*

As mentioned before, the cascade reaction of cellobiose conversion to gluconic acid involves two consecutive steps; cellobiose hydrolysis to glucose, followed by glucose oxidation to gluconic acid. In order to clarify the role of the support characteristics on the remarkable improvement of selectivity to gluconic acid in this tandem reaction, the aforementioned intermediate reactions were performed separately, using cellobiose or glucose as substrate. Firstly, the hydrolysis of cellobiose under oxygen was performed using pristine and functionalized supports without gold loading under the same reaction conditions. A control experiment was also made in the absence of the catalyst. It is well known that water at high temperatures and pressures can reversibly generate H^+ ions, which are capable to perform acid-catalyzed reactions, such as hydrolysis of cellulose [51]. In our experiments, the control reaction showed only 6.7% conversion of cellobiose with ≈100% selectivity to glucose, which demonstrates that the extent of autohydrolysis of cellobiose is rather limited under designated mild reaction conditions (418 K and 5 bar O_2). The changes of cellobiose conversion in time over different supports in the absence of gold are compared in Fig. 7. Upon addition of the supports, the cellobiose conversion increased to 44.5%, 42% and 25% on CX5.6, CX6.1 and OMC. Additionally, pristine CNT converted 26.4% of cellobiose, which agrees well with results reported previously under the same reaction conditions, but with extended reaction time to 3 h [5]. Hence, it is evidenced that all of the supports participated in the conversion of cellobiose. Moreover, the conversion of cellobiose further increased upon the introduction of Au nanoparticles, reaching 100% over Au/CX5.6_citric in 60 min of the reaction. This implies that Au is not only active in the glucose oxidation to gluconic acid, but also increases the overall conversion rate of cellobiose in this cascade process. This can be attributed to the shift of the kinetic equilibrium toward products, as a result of increased glucose conversion to gluconic acid, as well as the effect of more acidic pH of the reaction mixture. In addition, careful inspection of Fig. 7 shows that in the case of CNT, the conversion of cellobiose reaches a plateau after 60 min of the reaction which is in contrast to the results obtained using mesoporous carbon supports. Thus, it is evidenced for the first time that mesoporous carbons can outperform CNT in the cellobiose hydrolysis reaction and might be potentially useful for the hydrolysis of cellulose. It is also very important to point out that the conversion of cellobiose in hydrolysis increased with increasing pore size, but the difference between CX6.1 with average pore size of 9.2 nm and CX5.6 with 17, 25 nm is small. This observation suggests that the diffusion limitations in pores larger than 9 nm are less pronounced in the presence of mainly cellobiose in the reaction mixture. Hence, smaller diffusional limitations in bigger pores are not the only factor contributing to higher yields of gluconic acid obtained on Au/CX5.6 as compared to Au/CX6.1 (Fig. 6). In addition, it was demonstrated here that the presence of strong acidic groups which would definitely be necessary for the hydrolysis of cellulose under designated reaction conditions (418 K and 5 bar O_2) [2,52,53], are not mandatory when cellobiose is used as a substrate. It is noted that the hydrolysis of cellobiose readily took place on the pristine supports containing only very small amount of oxygenated groups (Table 2), which can suggest that this step is not rate determining in the overall cascade process.

Regarding functionalized supports, the observed drop in conversion of cellobiose as compared to their pristine counterparts (Fig. 7) can be attributed to the slightly decreased adsorption of cellobiose as a result of the competition with water molecules for the same active sites [59]. It is known that the adsorption of water increases with increased polarity of the carbon surface [54], or in other words hydrophilic surfaces have less affinity to cellobiose. Since, little attention is normally paid to the interaction between cellobiose and the catalyst, this effect is usually neglected. Nevertheless, it can strongly modify adsorption properties of carbons toward reactants and products in the tandem reaction involving molecules of various sizes and polarities.

Certainly, the extent of the secondary reactions which affect the catalyst selectivity in cellobiose oxidation to gluconic acid can be modified by the overall conversion degree. Hence, it is necessary to compare the catalysts' behaviors as a function of cellobiose conversion. Thus, the selectivity of the supports in hydrolysis was compared at cellobiose conversion of 25–30% and the results are shown in Supplementary material, Table 2s. In contrast to the literature reports dealing with the oxidative conversion of cellobiose to gluconic acid using CNT [5], TiO_2 [7] and polyoxometalates [6], in the present work we have observed gluconic acid among hydrolysis products, in the absence of Au particles. However, recently, gluconic acid was reported among products of glucose oxidation on MgO support [55]. The presence of gluconic acid among reaction products shows that carbon mesoporous supports studied here have ability to activate oxygen under the selected reaction conditions. Other products consisted of mainly glucose, glyceric and glycolic acid with trace amounts of acetic acid and oxalic acid. These side products originated from the decomposition of glucose [5,8]. It should be underlined that higher glucose selectivity was obtained using functionalized supports in comparison to the pristine ones. Clearly, Au supported on functionalized supports displayed higher rate of hydrolysis with respect to the non-catalytic decomposition of sugars (glucose/fructose) as evidenced in Fig. 6. These results show that the phenolic groups which were present in majority on

Table 6
The rate constants [h^{-1}] for each of the intermediate steps of oxidative conversion of cellobiose for supports and selected catalysts.

Catalyst	k_0	k_1	k_2	k_3	k_4	k_5	k_6
CX5.6	0.34	0.091	0.044	0.099	0.005	0.179	0
CX5.6_air	0.22	0.071	0.010	0.011	0.000	0.146	0
CX6.1	0.29	0.061	0.060	0.056	1.330	0.228	0
Cx6.1_air	0.21	0.079	0.079	0.000	0.000	0.171	0
OMC	0.27	0.312	0.085	0.051	5.800	0.081	0
OMC_air	0.17	0.079	0.069	0.032	0.079	0.144	0
Au/CX56_citric	3	0.69	2.3	60	2.1	0.18	0.0005
Au/CX56_citric_air	1.1	0.33	0.74	13	0	0.02	0
Au/CX6.1_IMP	1.45	0.7	0.76	17	0.37	0.12	0
Au/CX6.1_citric	1.5	0.82	0.68	15	0	0.058	0
Au/CX6.1_citric_air	1.2	1.1	0.69	24	0	0.098	0
Au/OMC_IMP	1.2	0.29	0.38	2.7	0.005	0.56	0
Au/OMC_air_IMP	0.91	0.37	0.41	28	0	0.15	0

the surface of the functionalized carbons as shown by the various techniques applied here (XPS, TPD and IR) were evidently involved in the selective hydrolysis of glycosidic linkages in cellobiose (see Fig. 5). On the other hand, higher concentrations of gluconic acid were observed on supports with smaller pore size, which can be attributed to inhibited diffusion and desorption of glucose from the pores leading to consecutive reactions. Interestingly, the best support, CX5.6_air, showed a small amount of gluconic acid and only traces of other products. This can be the result of faster release of glucose molecules from the catalysts surface and its inhibited readsorption on the support for further conversion/degradation.

The development of a simple kinetic model for stepwise reactions offers a practical way to compare the relative rates of competitive adsorptions (conversions) for different species on catalyst surfaces. Hence, taking into consideration the experimentally recorded changes in conversion versus time during oxidative conversion of cellobiose over supports and catalysts, a simplified catalytic model was established for the first time, which is shown in Fig. 8. The calculated rate constants for each of the steps for all supports and selected catalysts are summarized in Table 6. Reasonably good agreement was achieved between the values predicted by the model and those obtained experimentally, which is shown by the close fit of the modeled data (lines) and experimental results (points) in Supplementary material, Fig. 6s. A careful inspection of the k values listed in Table 6 together with the individual concentration versus time profiles revealed that k_0, the rate of disappearance of cellobiose, increased with the corresponding increase in mesopore size, regardless of the presence or absence of gold nanoparticles. In addition, the conversion of cellobiose increased with the addition of Au nanoparticles, as mentioned earlier. The functionalization of the supports resulted in an apparent decrease of over 30% in k_0 with regards to their pristine counterparts. The calculations also revealed that the rate constant of the oxidation of glucose to gluconic acid is zero (k_6 in Table 6), which means that the conversion of glucose to gluconic acid is likely to take place directly on the surface of the catalysts, without prior desorption of glucose to the solution followed by its readsorption for oxidation. In addition, comparing k_3 and k_4 (Table 6), which are the rate constants of the degradation of glucose and gluconic acid (Fig. 8) on the Au catalysts, it is evident that gluconic acid has much higher stability than glucose, regardless of the catalytic system. Furthermore, a higher rate of gluconic acid degradation (k_4) can be clearly observed on the pristine supports, where readsorption of gluconic acid is not hindered by the competitive adsorption of water.

The influence of the functional groups on the second step of this tandem process was also investigated. Thus, glucose oxidation was performed over Au/CX5.6_air_citric and Au/CX5.6_citric catalysts under the conditions described in detail in the experimental part. The oxidation of glucose on Au/CX5.6_citric showed 100% conversion in 90 min, with 4.3% selectivity to gluconic acid, which confirms that the oxidation of glucose to gluconic acid does not take place favorably in this catalytic system. Other products included: glycolic acid 2.0%, oxalic acid 3.2% and acetic acid 4.5%. In sharp contrast, Au/CX5.6_air_citric converted only 9.5% of glucose with 39.9% selectivity to gluconic acid. Other identified products were: glycolic acid 27%, acetic acid 0.5%, oxalic acid 6%. The measured changes of concentration in time recorded in glucose oxidation experiments were fitted to the reaction model shown in Fig. 8, with appropriate modifications. The calculated k_0 was

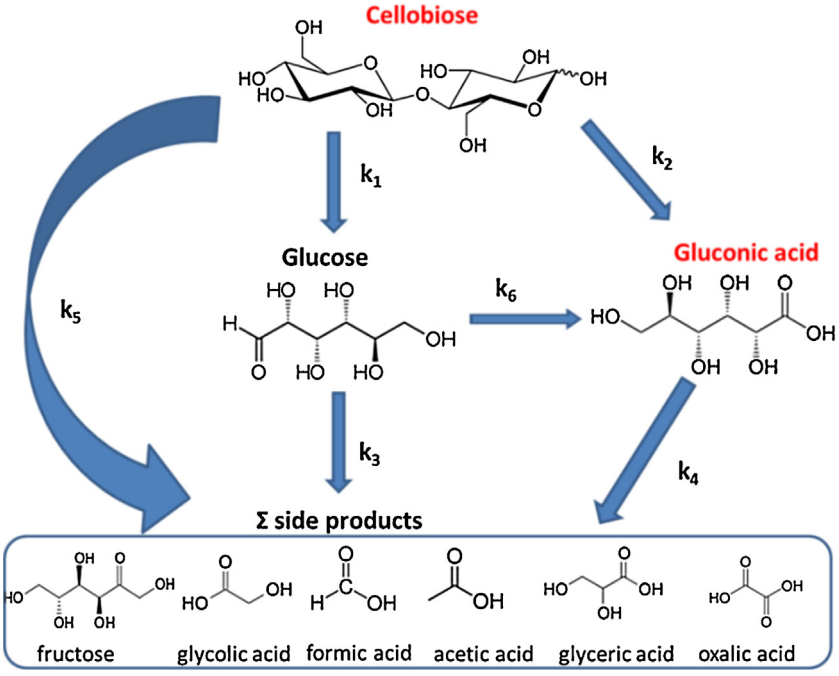

Fig. 8. A simplified kinetic model of oxidative conversion of cellobiose to gluconic acid.

two orders of magnitude higher for the Au supported on pristine support (2.46 vs 0.0026 [h^{-1}]). The notably lower rate constant on Au/CX5.6_air_citric as compared to that on Au/CX5.6_citric is clearly the result of impaired adsorption of glucose due to the aforementioned competition for active sites with water molecules on hydrophilic supports. Moreover, the calculations showed that decomposition of gluconic acid ($k_4 = 0$) does not take place on Au/CX5.6_air_citric, thus the side products come from decomposition of glucose in contrast to $k_4 = 0.83$ in case of Au/CX5.6_citric. Furthermore, since the selectivity of the tandem conversion of cellobiose to gluconic acid can be strongly affected by the degradation of gluconic acid, thus a separate set of reactions was conducted using gluconic acid as a substrate. The oxidation of gluconic acid was carried out using Au/OMC_IMP, Au/OMC_air_IM, Au/CX5.6_citric and Au/CX5.6_air_citric and a pronounced effect of the presence of phenolic groups on the surface of the mesoporous supports was observed. In 90 min, under the same reaction conditions, Au_OMC showed 63% conversion of the substrate as compared to only 22% obtained by Au_OMC_air. In comparison, Au/CX5.6 converted 90% of gluconic acid which decreased to as low as 17% when Au/CX5.6_air_citric was used. By far, it is evident that the presence of the phenolic groups drastically decreased the adsorption and further oxidation of gluconic acid, regardless of the pore size of the support. Thus, based on these results, two main effects of the functional groups can be established: (1) to make the support inert for degradation of gluconic acid and (2) to passivate supported gold to prevent gluconic acid overoxidation. Importantly, these effects significantly contribute to the overall selectivity to gluconic acid in the cascade reaction and can further explain the superb selectivity obtained by Au/CX5.6_air_citric catalyst in the present work (see Fig. 6). On the other hand, the 'free' carboxyl group of D-gluconic acid is known to be responsible for the poisoning of the active sites of the noble metal catalysts [48]. Our results apparently show that covering a substantial fraction of active sites on functionalized carbon supports by water molecules, substantially weakens the adsorption of D-gluconic acid onto the catalyst surface preventing catalyst deactivation and rendering remarkably high selectivity in the tandem process.

3.4.3. *Combined effect between the pore size and phenolic groups on the surface of mesoporous carbon in the tandem oxidative conversion of cellobiose to gluconic acid*

Phenolic groups introduced in the present work are known to be only weakly Brønsted acidic [56]. Despite that, a very high selectivity of almost 80% to gluconic acid was obtained using Au supported on this weakly acidic support. In addition, the selectivity to gluconic acid varied drastically in the present work within the supports having similar amounts of functional groups on the surface (compare Table 3 and Fig. 6). These results are in contrast to the literature reports concerning this tandem reaction, which underline that high selectivity to gluconic acid is directly correlated to the strength of acid sites present on the support, and increases with increased acidity [3,5,7]. A global analysis of our results strongly suggests that the selectivity to gluconic acid in this process cannot be attributed solely to the acid–base property of carbon, but it is rather influenced by a proper combination of chemistry of the surface and the texture of the mesoporous support.

The hydrolytic oxidation of cellobiose is a three-phase process, which evidently must be influenced to some extent by mass transfer limitations. It is worthwhile noting that the molecular sizes of cellobiose and glucose are 1.1 nm and 0.84 nm respectively, as calculated by Gaussian 03 (Gaussian 03, revision C.02. Wallingford, CT: Gaussian, Inc., 2004.). However, the hydrated radius of cellobiose in water is larger than the molecular size itself. Thus, on the supports having larger voids or mesopores, the reactant molecules can more rapidly diffuse into the mesopores of the catalyst and have sufficient contact with the Au nanoparticles, which may be one of the important factors accounting for the faster reaction rates on the supports with larger average mesopores size. It is also evident from our results that larger pore size favors a higher yield of gluconic acid by increasing the reaction rate without having a detrimental effect on selectivity from comparison of the results shown in Fig. 6 and Table 1s in Supplementary material. Au/CX5.6_citric with pore sizes of 15, 25 nm accounted for 43.5% yield of gluconic and 56.6% selectivity in 30 min as compared to Au/CX6.1_citric with a pore size of 9.2 nm which obtained 42% gluconic yield with 54.7% selectivity in 60 min. It is important to note that the conversion of cellobiose was similar for both catalysts, which suggests that the larger pore size not only decreases the diffusional limitations, but also affects the selectivity to glucose and subsequently to gluconic acid in the tandem process.

With respect to the chemistry of the supports, the addition of weakly acidic functional groups such as OH led to a remarkable increase in the selectivity toward gluconic acid (compare Au/CX5.6_air_citric obtained gluconic yield of 60.8%, with selectivity of 79.8% with the results of Au/CX5.6_citric mentioned above). Hence, it is worth noting that the functionalization of the carbon support led to over 20% increase in selectivity to gluconic acid, and the introduction of larger pores and functionalization led to a similar increase in selectivity, but obtained in 50% shorter reaction time. Thus, there is an evident combined effect of texture and the chemistry of the mesoporous carbon support on the catalysts performance in this tandem process.

It is further noted that the mesoporous carbons studied here have both hydrophilic sites, due to oxygenated functionalities, and hydrophobic regions, owing to the presence of aromatic frameworks. Cellulose also possesses both hydrophilic OH groups (in the equatorial plane of the glucose unit) and hydrophobic CH groups. Hence, carbons and cellulose can both exhibit hydrogen bonding and van der Waals forces, including weakly polarized interaction between CH groups of cellobiose and polyaromatic rings [56]. Reports in the literature show that the longer the glucan chain, the easier it adsorbs onto the surface of mesoporous carbon [52]. This suggests that the adsorption of cellobiose is indeed driven by the CH-π hydrophobic interaction between hydrogen in cellobiose and aromatic rings of the surface of the mesoporous carbon support. It follows that the adsorption of cellobiose on the carbon surface is stronger than that of glucose or gluconic acid, due to the larger number of CH groups present in its structure. These CH groups allow cellobiose to compete more effectively with water molecules on the functionalized polar supports [54]. This explains why there was only a slight drop in cellobiose conversion on Au supported on functionalized supports. On the contrary, it is known that the adsorption of monomers such as glucose or gluconic acid is strongly reduced on polar supports by competitive adsorption of water. This is in line with a very low conversion of the individual glucose and gluconic acid substrates observed in the present work on Au dispersed on functionalized supports. It should be noted that in case of the direct conversion of cellobiose to gluconic acid, it is critical for the adsorption of cellobiose to be preferred over the adsorption of glucose, because it ensures that the hydrolysis step proceeds selectively to glucose and its further oxidation. In this way, the extent of sequential side reactions resulting in degradation products is strongly diminished. Moreover, impeded adsorption of gluconic acid by cellobiose and water molecules on functionalized supports leads to further improvement in the overall selectivity of the cascade process, as it was evidenced in our results. In addition, it is known that the CH-π hydrophobic interaction of cellobiose and carbon is more energetically favorable on the defect sites of carbon [54], such as pores in our case. On the other hand, the adsorption of glucans within the confining mesopores of carbon is accompanied by a significant mechanical strain on the cellobiose molecule. In

turn, this mechanical strain is believed to facilitate hydrolysis since the excess energy can be relieved via glycosidic bond breaking [56]. Moreover, the conformational change is induced into glucan chains in the constrained position within mesopores, which makes the glycosidic bond more exposed for hydrolysis [54] assisted by water autoprotolysis [52]. In addition, weak acidic sites such as OH functionalities situated in the defect sites can be active in the hydrolysis of various length glucans generated from cellulose [57]. Hence, on the basis of the aforementioned literature findings and analysis of the results obtained here, it is evident that the adsorption of cellobiose on the surface of mesoporous carbon is affected by the average mesopores size of the support, which results in different catalytic selectivity and activity in direct conversion of cellobiose to gluconic acid.

Regarding the carbon xerogels, it can be deducted that the conformational change is induced on cellobiose within the bigger pores (support CX5.6), which makes the glycosidic bond more exposed. This would explain the higher selectivity to glucose obtained on carbon xerogels with larger average mesopores size. Moreover, on the pristine supports which have predominantly hydrophobic character, the adsorption of organic compounds is favored over the adsorption of water molecules, which is in line with higher reaction rates obtained on these supports in the present work. However, due to the same reason, the readsorption of glucose and gluconic acid onto the surface of these supports is facilitated, leading to their further conversion/degradation resulting in overall lower selectivity to the final product, as evidenced from the glucose and gluconic oxidation results described above.

Concerning the Au supported on functionalized carbons, the dual role of the OH groups can be certainly established. First of all, the in-plane weakly acidic OH functional groups can work as a conformational site by creating hydrogen bonds with constrained glycosidic oxygens, as previously reported in cellulose hydrolysis over functionalized amorphous carbon [58]. In the present work, the formation of this hydrogen bond is evidenced by the increased selectivity to glucose in cellobiose hydrolysis on functionalized supports versus pristine ones (Supplementary material, Table 2s). Further, it should be noted that the adsorption of glucose as a monomer of cellobiose was strongly inhibited on the Au/CX5.6_air, which supports the conclusion that glycosidic oxygen must participate in the adsorption of cellobiose on functionalized supports. The phenolic groups along with carboxylic acid groups that were also present on the surface of CX (Table 3) can also function as catalytic sites, by providing an additional proton source for cleaving glycosidic bonds. The activity of carboxylic and phenolic weak acid sites was recently demonstrated in hydrolysis of biomass derived miscanthus xylan to xylose [59]. Moreover, as it was evident from the analysis of our XPS results, the presence of functional groups on the surface influences the position of gold nanoparticles, coordinating them in close proximity to the phenolic groups which serve as coordination sites for cellobiose.

On the basis of our comparative study, the reaction mechanism for the tandem conversion of cellobiose to gluconic acid using Au supported on functionalized CX can be proposed. Hence, it is speculated that cellobiose is immobilized in the defect sites/pores on the surface of CX via CH-π electron interaction. Subsequently, additional strain is imposed on the cellobiose in the larger mesopores, leading to a change in its conformation, exposing the glycosidic bond. The glyosidic bond then interacts via hydrogen bonding with the phenolic groups localized in the mesopores. The phenolic groups play double role as coordinating site close to the active site (Au) and as catalytic sites to hydrolyze cellobiose selectively to glucose. Subsequently, glucose diffuses without desorption to the surface of gold particles situated in the vicinity of the pores (or partially blocking the pores as in case of CX5.6_air), where the final step of oxidation reaction takes place producing gluconic acid. This mechanism is further supported by the results from reaction modeling discussed in the previous paragraph (Table 6). Thus, it was demonstrated that mesoporous carbons such as carbon xerogels with optimized texture and surface chemistry can offer an alternative and inexpensive support to CNT for the preparation of catalysts for biomass conversion.

4. Conclusions

An active and highly selective bifunctional catalyst consisting of 1 wt% Au supported on functionalized carbon xerogel was developed for application in one pot tandem conversion of cellobiose to gluconic acid under mild reaction conditions. Phenolic groups were introduced into the structure of mesoporous carbons by simple acid-free oxidation in air and the resulting supported Au catalyst obtained remarkable selectivity of almost 80% to gluconic acid in only 75 min of the reaction. It was demonstrated here for the first time that the adequate support polarity (adsorption properties) and reactant accessibility (support porosity) are crucial factors which should be accounted for in the development of multifunctional catalysts. Hence, the excellent selectivity to gluconic acid obtained by Au/CX5.6_air_citric was ascribed to the following functions of the oxidized support: (1) the ability of the surface phenolic groups to guide the adsorption of cellobiose, attaching it to the surface and selectively catalyze its hydrolysis; (2) the ability of hydrophilic surface covered with phenolic groups to adsorb water, which effectively blocks the active sites for glucose and gluconic acid readsorption for further degradation/overoxidation reactions; (3) the ability of the larger pores to impose strain on cellobiose to change its conformation and to increase the exposure of the glycosidic bond. Overall, the present results open new possibilities to manipulate the catalytic performance of bifunctional catalysts in order to further increase the yield of desired products, and to make such processes commercially more competitive.

Acknowledgements

This work was financed by QREN, ON2 and FEDER (Projects NORTE-07-0124-FEDER-000015 and NORTE-07-0162-FEDER-000050), and co-financed by FCT and FEDER through COMPETE—Programa Operacional Factores de Competitividade (project PEst-C/EQB/LA0020/2013) and PT2020 Program (Project UID/EQU/50020/2013). Dr. C. M. Sá (CEMUP) is thanked for assistance with XPS analyses. Dr. M. Enterría (LSRE-LCM) is kindly acknowledged for providing ordered mesoporous carbons and R.P. Rocha (LSRE-LCM) is thanked for the aid in TPD analysis. K. Eblagon is grateful to FCT for the post-doctoral grant with reference number SFRH/BPD/110474/2015.

Appendix A. Supplementary data

Supplementary data associated with this article can be found, in the online version, at http://dx.doi.org/10.1016/j.apcatb.2015.10.011.

References

[1] L. Hu, L. Lin, Z. Wu, S. Zhou, S. Liu, Appl. Catal. B: Environ. 174–175 (2015) 225–243.
[2] S. Van de Vyver, J. Geboers, P.A. Jacobs, B.F. Sels, ChemCatChem 3 (2011) 82–94.
[3] J. Zhang, X. Liu, M.N. Hedhili, Y. Zhu, Y. Han, ChemCatChem 3 (2011) 1294–1298.
[4] P. Barbaro, F. Liguori, N. Linares, C.M. Marrodan, Eur. J. Inorg. Chem. 24 (2012) 3807–3823.
[5] X. Tan, W. Deng, M. Liu, Q. Zhang, Y. Wang, Chem. Commun. 46 (2009) 7179–7181.
[6] D. An, A. Ye, W. Deng, Q. Zhang, Y. Wang, Chem.—Eur. J. 18 (2012) 2938–2947.

[7] P.N. Amaniampong, K. Li, X. Jia, B. Wang, A. Borgna, Y. Yang, ChemCatChem 6 (2014) 2105–2114.
[8] P.N. Amaniampong, X. Jia, B. Wang, S.H. Mushrif, A. Borgna, Y. Yang, Catal. Sci. Technol. 5 (2015) 2393–2405.
[9] N. Mager, N. Meyer, A.F. Léonard, N. Job, M. Devillers, S. Hermans, Appl. Catal. B: Environ. 148–149 (2014) 424–435.
[10] A. Onda, T. Ochi, K. Yanagisawa, Catal. Commun. 12 (2011) 421–425.
[11] F. Rodríguez-Reinoso, Carbon 36 (1998) 159–175.
[12] M. Yabushita, H. Kobayashi, J.-Y. Hasegawa, K. Hara, A. Fukuoka, ChemSusChem 7 (2014) 1443–1450.
[13] P.V. Samant, F. Goncalves, M.M.A. Freitas, M.F.R. Pereira, J.L. Figueiredo, Carbon 42 (2004) 1321–1325.
[14] C. Alegre, M.E. Gálvez, R. Moliner, V. Baglio, A.S. Aricò, M.J. Lázaro, Appl. Catal. B: Environ. 147 (2014) 947–957.
[15] N. Job, M.F.R. Pereira, S. Lambert, A. Cabiac, G. Delahay, J.-F. Colomer, J. Marien, J.L. Figueiredo, J.-P. Pirard, J. Catal. 240 (2006) 160–171.
[16] S.A. Al-Muhtaseb, J.A. Ritter, Adv. Mater. 15 (2003) 101–114.
[17] R.W. Pekala, J. Mater. Sci. 24 (1989) 3221–3227.
[18] A.M.T. Silva, B.F. Machado, J.L. Figueiredo, J.L. Faria, Carbon 47 (2009) 1670–1679.
[19] M. Enterría, M.F.R. Pereira, J.I. Martins, J.L. Figueiredo, Carbon 95 (2015) 72–83.
[20] J. Turkevich, P.C. Stevenson, J. Hillier, Discuss. Faraday Soc. 11 (1951) 55–75.
[21] J.L. Figueiredo, M.F.R. Pereira, M.M.A. Freitas, J.J.M. Órfão, Ind. Eng. Chem. Res. 46 (2007) 4110–4115.
[22] J.L. Figueiredo, M.F.R. Pereira, M.M.A. Freitas, J.J.M. Órfão, Carbon 37 (1999) 1379–1389.
[23] K.A. Morawa Eblagon, S.C.E. Tsang, Appl. Catal. B: Environ. 160–161 (2014) 22–34.
[24] K.A. Morawa Eblagon, K. Tam, K.M.K. Yu, S.C.E. Tsang, J. Phys. Chem. C 116 (2012) 7421–7429.
[25] J.A. Nelder, R. Mead, Comput. J. 7 (1965) 308–313.
[26] N. Job, R. Pirard, J. Marien, J.-P. Pirard, Carbon 42 (2004) 619–628.
[27] E. Antolini, Appl. Catal. B: Environ. 88 (2009) 1–24.
[28] N. Mahata, M.F.R. Pereira, F. Suárez-García, A. Martínez-Alonso, J.M.D. Tascón, J.L. Figueiredo, J. Colloid Interface Sci. 324 (2008) 150–155.
[29] S. Gil, M. Marchena, C.M. Fernández, L. Sánchez-Silva, A. Romero, J.L. Valverde, Appl. Catal. A: Gen. 450 (2013) 189–203.
[30] C. Lin, J.A. Ritter, Carbon 35 (1997) 1271–1278.
[31] C. Alegre, M.E. Gálvez, E. Baquedano, R. Moliner, E. Pastor, M.J. Lázaro, J. Phys. Chem. C 117 (2013) 13045–13058.
[32] A.G. Gonçalves, J.L. Figueiredo, J.J.M. Órfão, M.F.R. Pereira, Carbon 48 (2010) 4369–4381.
[33] J.L. Figueiredo, M.F.R. Pereira, Catal. Today 150 (2010) 2–7.
[34] G. Barco, A. Maranzana, G. Ghigo, M. Causà, G. Tonachini, J. Chem. Phys. 125 (2006), 1947061–12.
[35] S. Reiche, R. Blume, X.C. Zhao, D. Su, E. Kunkes, M. Behrens, Carbon 77 (2014) 175–183.
[36] R. Alamillo, M. Tucker, M. Chia, Y. Pagan-Torres, J. Dumesic, Green Chem. 14 (2012) 1413–1419.
[37] M. Takaoka, H. Yokokawa, N. Takeda, Appl. Catal. B: Environ. 74 (2007) 179–186.
[38] L. Stobinski, B. Lesiak, L. Kövér, J. Tóth, S. Biniak, G. Trykowski, J. Judek, J. Alloys Compd. 501 (2010) 77–84.
[39] C. Moreno-Castilla, F. Carrasco-Marín, A. Mueden, Carbon 35 (1997) 1619–1626.
[40] C. Alegre, M.E. Gálvez, E. Baquedano, E. Pastor, R. Moliner, M.J. Lázaro, Int. J. Hydrogen Energy 37 (2012) 7180–7191.
[41] R.P. Rocha, A.M.T. Silva, G. Dražić, M.F.R. Pereira, J.L. Figueiredo, Mater. Lett. 66 (2012) 64–67.
[42] X. Wang, N. Li, J.A. Webb, L.D. Pfefferle, G.L. Haller, Appl. Catal. B: Environ. 101 (2010) 21–30.
[43] R. Burgess, C. Buono, P.R. Davies, R.J. Davies, T. Legge, A. Lai, R. Lewis, D.J. Morgan, N. Robinson, D.J. Willock, J. Catal. 323 (2015) 10–18.
[44] J.L. Figueiredo, M.F.R. Pereira, J. Energy Chem. 22 (2013) 195–201.
[45] L. Prati, G. Martra, Gold Bull. 32 (1999) 96–101.
[46] F. Porta, L. Prati, J. Catal. 224 (2004) 397–403.
[47] J.J. Verendel, T.L. Church, P.G. Andersson, Synthesis 11 (2011) 1649–1677.
[48] A. Abbadi, H. van Bekkum, J. Mol. Catal. A: Chem. 97 (1995) 111–118.
[49] Y. Önal, S. Schimpf, P. Claus, J. Catal. 223 (2004) 122–133.
[50] P. Qi, S. Chen, J. Chen, J. Zheng, X. Zheng, Y. Yuan, ACS Catal. 5 (2015) 2659–2670.
[51] C. Luo, S. Wang, H. Liu, Angew. Chem. 119 (2007) 7780–7783.
[52] A. Cabiac, E. Guillon, F. Chambon, C. Pinel, F. Rataboul, N. Essayem, Appl. Catal. A: Gen. 402 (2011) 1–10.
[53] D. Yamaguchi, M. Kitano, S. Suganuma, K. Nakajima, H. Kato, M. Hara, J. Phys. Chem. C. 113 (2009) 3181–3188.
[54] G.S. Foo, C. Sievers, ChemSusChem 8 (2015) 534–543.
[55] P.J. Miedziak, H. Alshammari, S.A. Kondrat, T.J. Clarke, T.E. Davies, M. Morad, D.J. Morgan, D.J. Willock, D.W. Knight, S.H. Taylor, G.J. Hutchings, Green Chem. 16 (2014) 3132–3141.
[56] O.M. Gazit, A. Katz, J. Am. Chem. Soc. 135 (2013) 4398–4402.
[57] A. Charmot, P.-W. Chung, A. Katz, ACS Sustain. Chem. Eng. 2 (2014) 2866–2872.
[58] S. Suganuma, K. Nakajima, M. Kitano, D. Yamaguchi, H. Kato, S. Hayashi, M. Hara, J. Am. Chem. Soc. 130 (2008) 12787–12793.
[59] P.W. Chung, A. Charmot, O.A. Olatunji-Ojo, K.A. Durkin, A. Katz, ACS Catal. 4 (2014) 302–310.